Fast simultaneous seismic source separation using Stolt migration and demigration operators

Amr Ibrahim[*†] **and Mauricio D. Sacchi**[*]

[*] *Department of Physics, University of Alberta, Edmonton, AB, T6G 2E1, Canada*

[†] *Department of Physics, Faculty of Science, Beni Suef University, Beni Suef, Egypt.*

(May 19, 2015)

GEO-2015-0044.R1

Running head: **Source separation using Stolt migration**

ABSTRACT

Stolt migration is a Fourier domain imaging operator that assumes a constant velocity media. In this article, we adopt a multi-velocity version of the Stolt migration and demigration operators to derive a transform that can decompose seismic data into a sparse collection of coefficients in image space. This Stolt-based transform is similar to the Apex Shifted Hyperbolic Radon Transform (ASHRT). However, the Stolt-based transform is considerably faster than the classical ASHRT because it uses two fast operators (forward and inverse Fast Fourier Transforms) to estimate the data coefficients in image space.

We use this Stolt-based transform as a tool for simultaneous seismic source separation by removing erratic interference noise in common receiver gathers. Estimating the coefficients of interference-free seismic data using the Stolt-based transform is posed as an inverse problem. The solution of this inverse problem is found by minimizing a cost function which includes a sparsity promoting regularization term. Additionally, the cost function incorporates a robust misfit function that is not sensitive to erratic interferences. Our tests

on synthetic and field data examples show that this new transform can efficiently remove interference noise and achieve fast simultaneous seismic source separation.

INTRODUCTION

Hydrocarbon exploration requires accurate subsurface imaging which usually uses seismic reflection data. Seismic reflection data are collected by firing artificial seismic sources at or near the surface. Seismic source waves are reflected at the boundaries between different geological formations and are recorded by an array of seismic sensors (receivers) at the surface (Yilmaz, 2001). This seismic experiment is repeated by moving the location of the source and/or receivers to explore more of the subsurface. Classical seismic exploration requires a long time interval between sources firing times to avoid source interferences. This long time interval between sources firing times increases the total acquisition time and thereby increases the acquisition cost. This also restrict the spatial density of the source distribution and thereby limits subsurface illumination. Limited seismic illumination is especially problematic for imaging deep subsalt structures (Michell et al., 2006). The aim of simultaneous seismic source acquisition is to decrease the total acquisition time by shortening the time interval between sources (Garotta, 1983; Beasley, 2008; Berkhout, 2008; Ikelle, 2010). This introduces source interferences and processing techniques are needed to separate sources prior to applying conventional data processing flows that rely on a single source assumption.

Separation methods assume that simultaneous seismic source data can be modelled from individual seismic sources data (Berkhout, 2008). For instance, if we let $\mathbf{D}$ represent the data of all seismic sources arranged into a cube and $\mathbf{b}$ represents the two dimensional simultaneous seismic source data, then

$$\mathbf{b} = \Gamma\ \mathbf{D}, \tag{1}$$

where Γ represents the blending operator that contains the source firing times (Berkhout,

2008). Therefore, simultaneous seismic source data $\mathbf{b}$ can be simply separated by compensating for the source firing time delay followed by the subdivision of the data into individual source segments. This is equivalent to applying the adjoint of the blending operator Γ to the simultaneous seismic source data $\mathbf{b}$. This operation is often called pseudo-deblending (Berkhout, 2008)

$$\widetilde{\mathbf{D}} = \Gamma^T \mathbf{b}, \tag{2}$$

where $\widetilde{\mathbf{D}}$ represents the pseudo-deblended data cube. However, pseudo-deblending does not remove source interference as shown in Figure 1. Therefore, a more advanced processing technique is needed for simultaneous seismic source separation.

[Figure 1 about here.]

Current simultaneous seismic source separation (or commonly known as deblending) methods can be classified into two broad categories. In the first category, deblending is posed as an inversion problem where the non-overlapping data are estimated by minimizing a cost function. These methods estimate the non-overlapping data by estimating the data coefficients in a transform domain. If a suitable transform is chosen, the non-overlapping data can be represented by a sparse collection of coefficients in the transform domain. Therefore, sparse inversion strategies can be used to estimate the coefficients that represent the unknown deblended data. Simultaneous seismic source separation methods that belong to this category include sparse Radon inversion (Moore et al., 2008; Akerberg et al., 2008), iterative $\omega - k$ filtering (Mahdad et al., 2011; Doulgeris et al., 2012), iterative rank reduction (Cheng and Sacchi, 2013), curvelet inversion (Lin and Herrmann, 2009; Wason et al., 2011) and projected gradient optimization algorithms (Abma et al., 2010).

The second category of simultaneous seismic source separation methods contain al-

gorithms that use denoising techniques to remove source interferences from the pseudo-deblended data (Kim et al., 2009; Huo et al., 2012; Trad et al., 2012; Ibrahim and Sacchi, 2014c,b,a; Sacchi, 2014). These denoising methods utilize the incoherency of sources in common receiver gathers. This incoherency results from random time delays (also known as dithering) in the firing times of the sources (Moore et al., 2008). For example, the front of the data cube in Figure 2 shows a group of seismic traces that belong to one source location which is called common source gather.

[Figure 2 about here.]

The source interferences have coherent structure in common source gathers and it is difficult to distinguish source interferences from seismic reflections. However, the cube side in Figure 2 shows seismic traces that belong to one receiver location (common receiver gather) where the source interferences are incoherent events while reflections are coherent events. Therefore, source interferences can be removed by denoising common receiver gathers of simultaneous seismic source data. Sparsity of the seismic data in a transform domain such as Radon (Sacchi and Ulrych, 1995a), Fourier (Sacchi et al., 1998) or Curvelet (Herrmann and Hennenfent, 2008) can be used for estimating common receiver gathers that are free from interference noise. Unlike the inversion approach, the denoising approach avoids the repetitive computation of the blending/pseudo-deblending operators associated with the minimization of a cost function. Therefore, the denoising methods can separate the simultaneous seismic source data faster than the inversion methods. Recently, Ibrahim and Sacchi (2014c) introduced a simultaneous seismic source separation method that uses a robust Apex Shifted Hyperbolic Radon Transform (ASHRT) denoising. The ASHRT transform was used because its basis functions closely resemble the seismic reflections in common

receiver gathers. However, the ASHRT transform has a high computational cost since it models the data by summation over three parameters (zero offset time, apex location and velocity). To speed up the ASHRT computation for seismic data interpolation, Trad (2003) proposed using the Stolt migration operator. Stolt (1978) introduced this operator to compute the subsurface image of a constant velocity media by mapping the data in Fourier domain and using Fast Fourier Transforms (FFT). In this work, we use the Stolt-based transform to focus the seismic reflection data into a sparse collection of coefficients in the transform domain. Therefore, this fast Stolt-based transform can be used to remove seismic source interference and achieve faster simultaneous seismic source separation.

THEORY

Robust Radon Transform

Denoising common receiver gathers requires a transform that focuses reflections while attenuating the incoherent source interferences. Since seismic reflections are approximated by hyperbolas, a transform that uses hyperbolic basis functions should be suitable for denoising seismic data. Transforms that use hyperbolic basis are variants of the classical Radon transform (Radon, 1917; Beylkin, 1987). The most common of these transforms is the hyperbolic Radon transform used for processing common midpoint gathers where all the apexes of seismic reflection hyperbolas are usually located at zero offset. However, seismic reflection hyperbolas in common receiver gathers are not centred at zero offset for dipping subsurface layers (Trad, 2003; Ibrahim and Sacchi, 2014c).

Denoising using ASHRT assumes that a seismic reflection data can be modelled using

a superposition of apex shifted hyperbolas as follows

$$d(t,h) = \sum_{a_{min}}^{a_{max}} \sum_{v_{min}}^{v_{max}} m(\tau = \sqrt{t^2 - \frac{(h-a)^2}{v^2}}, v, a) \tag{3}$$

where $d(t,h)$ is the modelled seismic data, $m(\tau, v, a)$ is the ASHRT model, t is time, h is receiver offset and v is velocity. The parameters τ and a represent the reflection hyperbola apex time (zero offset time) and apex location, respectively. The ASHRT model can be estimated using the adjoint operation as follows

$$\widetilde{m}(\tau, v, a) = \sum_{h_{min}}^{h_{max}} d(t = \sqrt{\tau^2 + \frac{(h-a)^2}{v^2}}, h) \tag{4}$$

where $\widetilde{m}(\tau, v, a)$ is the estimated ASHRT model. These transforms can be rewritten in the operator format as

$$\mathbf{d} = \mathbf{L}\mathbf{m}, \tag{5}$$

$$\widetilde{\mathbf{m}} = \mathbf{L}^T\mathbf{d}, \tag{6}$$

where $\mathbf{d}$, $\mathbf{m}$ and $\widetilde{\mathbf{m}}$ represent the data, model and estimated model in vector form, respectively. The forward and adjoint ASHRT operators are represented by $\mathbf{L}$ and $\mathbf{L}^T$, respectively. The estimated model $\widetilde{\mathbf{m}}$ and the original model $\mathbf{m}$ are not the same because Radon transforms are not orthogonal transformations ($\mathbf{L}\mathbf{L}^T \neq 1$). Furthermore, seismic reflection data usually have significant noise, missing traces and limited spatial range for recorded traces. All these factors contribute to lowering the resolution of the model estimated by the adjoint Radon operator. Therefore, Thorson and Claerbout (1985) suggested casting the problem of Radon model estimation as an inversion problem. This requires a regularization (penalty) term in the cost function that is used to estimate the Radon model. The general form of the cost function that one minimizes to obtain the Radon coefficients is given by

(Trad et al., 2003)

$$J = \|\mathbf{d} - \mathbf{L}\,\mathbf{m}\|_p^p + \mu\|\mathbf{m}\|_q^q \tag{7}$$

$$= \|\mathbf{r}\|_p^p + \mu\|\mathbf{m}\|_q^q$$

where μ is the tradeoff parameter that controls the relative weight between the model regularization term $\|\mathbf{m}\|_q^q$ and the misfit between the observed and modelled data term $\|\mathbf{r}\|_p^p$. The parameters p and q in the cost function represent the norms used to measure the misfit term and the model regularization term, respectively. For the model regularization term, the ℓ_2 norm ($q = 2$) is the conventional option. The advantage of using the ℓ_2 norm is that the cost function can be easily minimized by solving a linear system of equations. However, an ℓ_2 regularization results in smooth (low resolution) Radon models (Sacchi and Ulrych, 1995a,b). Since we choose Radon basis functions that closely match reflection hyperbolas, the ideal solution of Radon coefficients should be sparse. In regards to the misfit term in equation 7, the ℓ_2 norm ($p = 2$) is the conventional option. The ℓ_2 norm misfit is suitable when the misfit between the observed and modelled data follows a Gaussian distribution (Huber, 2011). However, simultaneous seismic source data usually have high amplitude reflections of one seismic source overlapping with low amplitude reflections of another seismic source.

[Figure 3 about here.]

Figure 3 shows a close up of a common receiver gather from Gulf of Mexico field data where such high amplitude interferences almost obscure the low amplitude reflections. The large outliers due to this strong interferences will degrade the accuracy of the models estimated using an ℓ_2 norm misfit. In order to minimize the influence of outliers, Claerbout and Muir

(1973) suggested replacing the conventional ℓ_2 norm misfit with an ℓ_1 norm misfit to make the inversion robust with respect to erratic noise (robust inversion) (Guitton and Symes, 2003; Ji, 2006, 2012). Ibrahim and Sacchi (2014c,b,a) proposed using this robust inversion technique for the simultaneous seismic source separation problem.

Equation (7) is minimized using the Iteratively Re-weighted Least Squares (IRLS) algorithm (Daubechies et al., 2010) for non-quadratic norms (p and/or $q \neq 2$) where

$$\|\mathbf{x}\|_p^p = \sum_i |x_i||x_i|^{p-2}|x_i| = \|\mathbf{W_x}\,\mathbf{x}\|_2^2 \tag{8}$$

where $\mathbf{x}$ is the vector to measure its norm (such as $\mathbf{r}$ and $\mathbf{m}$) and $\mathbf{W_x}$ is the weighting matrix defined as

$$[\mathbf{W_x}]_{ii} = |x_i|^{(p-2)/2} \quad 0 < p \leq 2 \tag{9}$$

Since this weighting matrix cannot be computed for $x_i = 0$, we redefine the weighting matrix for the model term $\mathbf{m}$ as follows

$$[\mathbf{W_m}]_{ii} = \begin{cases} \frac{1}{\sqrt{|m_i|^{2-p}}} & \text{if } m_i > \epsilon_m, \\ \frac{1}{\sqrt{\epsilon_m^{2-p}}} & \text{if } m_i \leq \epsilon_m\,. \end{cases} \tag{10}$$

Similarly, we redefine the weighting matrix for the misfit term as follows

$$[\mathbf{W_r}]_{ii} = \begin{cases} \frac{1}{\sqrt{|r_i|^{2-q}}} & \text{if } r_i > \epsilon_r, \\ \frac{1}{\sqrt{\epsilon_r^{2-q}}} & \text{if } r_i \leq \epsilon_r\,. \end{cases} \tag{11}$$

Both ϵ_r and ϵ_m represent small numbers to avoid the singularity at $r = 0$ and $m = 0$. Holland and Welsch (1977) estimated the optimal value of ϵ_r as

$$\epsilon_r = b_r \;\; \frac{\text{MAD}(\mathbf{r})}{0.6745}, \tag{12}$$

where MAD indicates the median absolute deviation of the residuals $\mathbf{r}$. The parameter b_r is a tuning parameter with recommended value $b_r = 1.345$. The parameter ϵ_m is computed

via the following expression

$$\epsilon_m = b_m \ \frac{max(|\mathbf{m}|)}{100}$$

where b_m is a tuning parameter that is related to the level of model sparsity (Guitton and Symes, 2003; Ji, 2006, 2012). We have converted the non-quadratic cost function into a sequence of quadratic minimization problems for fixed weighting matrices $\mathbf{W}_r$ and $\mathbf{W}_m$. Equation 7 can be rewritten in its standard form (Hansen, 1998) by a simple change of variable $\mathbf{u} = \mathbf{W}_m\mathbf{m}$

$$J = \|\mathbf{W}_r\left[\mathbf{L}(\mathbf{W}_m)^{-1}\mathbf{u} - \mathbf{d}\right]\|_2^2 + \mu\|\mathbf{u}\|_2^2. \tag{13}$$

This new cost function is minimized by the method of conjugate gradients (Scales, 1987) followed by the updating of the weighting matrices $\mathbf{W_r}$ and $\mathbf{W_m}$. We follow the method described by Trad et al. (2003) where the regularization term in equation (13) is omitted by setting $\mu = 0$. In this case, the number of conjugate gradient iterations plays the role of a trade-off parameter (Hansen, 1998). In our implementation, the IRLS internal conjugate gradient iterations are stopped when the misfit change between iterations is less than 0.01% (Ibrahim and Sacchi, 2014c).

Stolt-based Transform

The Stolt migration method is considered to be the fastest migration algorithm (Margrave, 2001). This operator performs migration by mapping data in the $\omega - k$ domain to vertical wavenumber k_z for a constant subsurface velocity. Despite of not being widely used any more in seismic imaging due to its constant velocity limitation, the low computational cost of the Stolt operator made it a useful tool in other fields such as medical imaging (Cafforio et al., 1991; Bamler, 1992; Garcia et al., 2013) and synthetic aperture radar imaging (Li

et al., 2014; Wu et al., 2014).

Using the exploding reflector principle (Claerbout, 1985) and a constant velocity assumption, the Stolt operator can be used to estimate the subsurface model from zero offset data. This estimated model $\widetilde{m}(\tau, v, x)$ is related to the data recorded at the surface $d(t, x)$ by the following relationship (Yilmaz, 2001)

$$\widetilde{m}(\tau, v, x) = \int\int d(\omega, k_x)\ \exp[-ik_x x - i\omega_\tau(v)\tau]\ d\omega\ dk_x \tag{14}$$

where x represents the horizontal axis and ω_τ is the Fourier dual of the apex time τ which is a function of the velocity through the modified dispersion relationship (Yilmaz, 2001)

$$\omega_\tau = \sqrt{\omega^2 - (vk_x)^2} \tag{15}$$

Equation 14 can be rewritten by changing the integration variable from ω to ω_τ

$$\begin{aligned}\widetilde{m}(\tau, v, x) = &\int\int C\ d(\omega = \sqrt{\omega_\tau^2 + (vk_x)^2}, k_x) \\ &\times \exp\left[-ik_x x - i\omega_\tau(v)\tau\right]\ d\omega_\tau\ dk_x\end{aligned} \tag{16}$$

where $C = \omega_\tau/\omega$ is a scaling factor resulting from the change of variables.

[Figure 4 about here.]

Figure 4 shows the steps required to image with the Stolt operator. Similarly, the forward Stolt modeling operator can be written as

$$\begin{aligned}d(t, x) = &\int\int\int m(\omega_\tau = \sqrt{\omega^2 - (vk_x)^2}, v, k_x) \\ &\times \exp[ik_x x + i\omega t]\ d\omega\ dk_x\ dv\end{aligned} \tag{17}$$

The forward and adjoint transforms in equations (16) and (17) can be written in operator form as follows

$$\mathbf{L}^T = \mathbf{FFT}^{-1}_{\omega_\tau, k_x}\ \mathbf{M}^T_{\omega, v, k_x}\ \mathbf{FFT}_{t,x}\ \mathbf{S}^T, \tag{18}$$

$$\mathbf{L} = \mathbf{S}\ \mathbf{FFT}^{-1}_{\omega,k_x}\ \mathbf{M}_{\omega_\tau,v,k_x}\ \mathbf{FFT}_{\tau,x}, \tag{19}$$

where, $\mathbf{FFT}$ is the Fast Fourier Transform, $\mathbf{M}_{\omega_\tau,v,k_x}$ is the Stolt mapping operator and $\mathbf{S}$ is a summation operator and its adjoint is a spraying operator (Claerbout, 1985). Although the Stolt operator is derived with a constant velocity assumption, it can be used to construct an equivalent of the ASHRT model with multiple velocities. Since each image represents one plane inside the ASHRT model cube at constant velocity, the ASHRT model is collection of all these images. Therefore, the adjoint Stolt operator in equation 18 includes a spreading operator $\mathbf{S}^T$ that computes several images with different velocities from the same data while the forward Stolt operator in equation 19 uses a summation operator to model the data.

The classical ASHRT operator has a computational cost of $O(n_a \times n_\tau \times n_v \times n_x)$, where n_a, n_τ, n_v and n_x are the number of apex locations, zero offset times, velocities and offsets, respectively. Assuming that we scan for all possible apex locations and times, then $n_a = n_x$ and $n_\tau = n_t$. Therefore, the ASHRT operator cost is $O(n_x^2 \times n_t \times n_v)$. On the other hand, the Stolt based ASHRT (without FFT zero padding) operator has a cost that is of the 2D FFT of the data with size $n_t \times n_x$ followed by $\omega - k$ mapping and inverse 2D FFT of the model with size $n_t \times n_v \times n_x$. Therefore, the total computational cost of an ASHRT implemented via the Stlot operator is $O([n_t \log_2(n_t) + n_x \log_2(n_x)][n_v + 1] + n_v \times n_{kx} \times n_\omega)$, where n_{k_x} and n_ω are the number of horizontal wavenumbers and temporal frequencies, respectively. In the previous analysis, we have assumed that both the data and the model are regularly sampled in space and apex, respectively. The latter permits us to adopt the computationally efficient FFT operators. However, if the data and/or the model are not regularly sampled, the FFT operator will be replaced by the less efficient discrete Fourier transform (DFT). The cost of the $\omega - k$ mapping is proportional to $n_v \times n_{k_x} \times n_\omega$ and we stress that the latter is an upper limit, since in practice we only scan for a limited group

of positive frequencies and use the Fourier domain symmetries to compute the negative frequencies.

[Figure 5 about here.]

Figure 5a shows the computational times of the conventional ASHRT and the Stolt-based ASHRT with and without zero padding. Zero padding is required to reduce artifacts associated with $\omega - k$ interpolation and improve Stolt mapping precision. Figure 5b shows the improvement in the computational time by using the Stolt-based ASHRT operator with and without zero padding compared to the conventional ASHRT. It is clear that using the Stolt operator can lead to significant savings in computational cost. Therefore, this operator can be useful in early stages of processing for quality control and velocity analysis. This is very important for processing large data sets that contain large number of common receiver gathers.

EXAMPLES

Synthetic Example

We initially tested simultaneous seismic source separation using numerically blended simple synthetic data example. The synthetic data was modeled using the Stolt-based forward ASHRT operator. It represents twelve reflections with velocities range from 4000 to 5000 ft/s and different apex shifts. We used the forward operator to model the synthetic data in order to test the ideal situation where the data are composed of apex shifted hyperbolas. The data are numerically blended with a 50% reduction in total acquisition time compared to conventional acquisition.

[Figure 6 about here.]

The firing times of both the conventional and blended sources are shown in Figure 6. The blending scheme simulates a single source moving in the same direction while firing with small random perturbations to the time interval between shots. The receivers are assumed to be at a fixed location similar to the case of ocean bottom nodes (OBN) or ocean bottom cables (OBC) acquisition.

[Figure 7 about here.]

[Figure 8 about here.]

[Figure 9 about here.]

A pseudo-deblended common receiver gather is shown in Figure 7a, the data recovered by forward modeling the estimated ASHRT model are shown in Figure 7b and the error in the recovered data is shown in Figure 7c. Four velocity panels of the estimated ASHRT model are shown in Figure 8. Each of these panels represents a constant velocity cross-section of the ASHRT model cube. These panels shows that hyperbolic reflections with different apex locations can be focused using the ASHRT transform. After eliminating interferences from all common receiver gathers, the deblended data cube is recovered as shown in Figure 9. The quality of deblending is measured in dB using the following formula

$$Q = 10\ log_{10}\left(\frac{\|\mathbf{d}_{original}\|_2^2}{\|\mathbf{d}_{original} - \mathbf{d}_{recovered}\|_2^2}\right). \tag{20}$$

where is $\mathbf{d}_{original}$ is the original unblended data and $\mathbf{d}_{recovered}$ is the deblended data recovered from the ASHRT models estimated by inversion. If $Q = 10$ dB, the ℓ_2 norm of the original data is 10 times larger than the error of the deblended data. Generally, values of

Q above 10 dB are considered acceptable deblending results. The Q value for the synthetic example is 22.01 dB.

Field Data Example

We tested simultaneous source separation with a numerically blended marine data example from the Gulf of Mexico. Similar to the synthetic example, the data are numerically blended with a 50% reduction in the total acquisition time. The source firing times versus source location for the first thirty sources are displayed in Figure 10. A pseudo-deblended common receiver gather is shown in Figure 11a, the data recovered by forward modeling the estimated ASHRT model is shown in Figure 11b and the error in the recovered data is shown in Figure 11c.

[Figure 10 about here.]

[Figure 11 about here.]

[Figure 12 about here.]

[Figure 13 about here.]

The Q value for the recovered common receiver gather is 12.63 dB. Four velocity panels of the estimated model are shown in Figure 12. After eliminating interferences from all common receiver gathers, the deblended data cube is retrieved and is shown in Figure 13. For the field data example, imposing a strict sparsity constraint is not a simple task. The reflection hyperbola generated by the Stolt operator do not exactly match the reflection hyperbolas in the data. This mismatch results from the approximated and coarse velocities

that are used in the transform and by the presence of amplitude versus offset (AVO) changes which are not included in the ASHRT operator. Therefore, the ASHRT transform does not focus reflections to sharp points and the estimated ASHRT model is not as sparse as the one obtained when using simple synthetic examples (Ibrahim and Sacchi, 2014c). Additionally, field data could suffer from missing near offset, irregular sampling and feathering which will reduce the operator ability to focus seismic reflections.

CONCLUSION

We have implemented a fast Stolt-based transform that is similar to the Apex shifted Hyperbolic Radon Transform (ASHRT) to remove source interferences in common receiver gathers of simultaneous seismic sources data. We showed that the Stolt-based transform can remove source interferences in common receiver gathers at a computational cost that is substantially below the computational cost of the classical ASHRT and with quality comparable to the classical ASHRT. Since the Stolt operator is implemented in the $\omega - k$ domain, it can be used in combination with the non-uniform Fourier transform to interpolate missing traces. Future work entails generalizing the transform to the 3D shot distribution.

ACKNOWLEDGMENTS

The authors are grateful to the sponsors of Signal Analysis and Imaging Group (SAIG) at the University of Alberta. This research was also supported by the Natural Sciences and Engineering Research Council of Canada via a grant to MDS.

REFERENCES

Abma, R., T. Manning, M. Tanis, J. Yu, and M. Foster, 2010, High quality separation of simultaneous sources by sparse inversion: 72nd Annual International Conference and Exhibition, EAGE, Expanded Abstracts, B003.

Akerberg, P., G. Hampson, J. Rickett, H. Martin, and J. Cole, 2008, Simultaneous source separation by sparse Radon transform: 78th Annual International Meeting, SEG, Expanded Abstracts, 2801–2805.

Bamler, R., 1992, A comparison of range-doppler and wavenumber domain sar focusing algorithms: Geoscience and Remote Sensing, IEEE Transactions on, **30**, 706–713.

Beasley, C. J., 2008, A new look at marine simultaneous sources: The Leading Edge, **27**, 914–917.

Berkhout, A., 2008, Changing the mindset in seismic data acquisition: The Leading Edge, **27**, 924–938.

Beylkin, G., 1987, Discrete Radon transform: Acoustics, Speech and Signal Processing: IEEE Transactions on, **35**, 162–172.

Cafforio, C., C. Prati, and F. Rocca, 1991, Sar data focusing using seismic migration techniques: Aerospace and Electronic Systems, IEEE Transactions on, **27**, 194–207.

Cheng, J., and M. D. Sacchi, 2013, Separation of simultaneous source data via iterative rank reduction: 83rd Annual International Meeting, SEG, Expanded Abstracts, 88–93.

Claerbout, J., and F. Muir, 1973, Robust modeling with erratic data: Geophysics, **38**, 826–844.

Claerbout, J. F., 1985, Imaging the earth's interior: Blackwell Scientific Publications Inc.

Daubechies, I., R. DeVore, M. Fornasier, and C. S. Gntrk, 2010, Iteratively reweighted least squares minimization for sparse recovery: Communications on Pure and Applied

Mathematics, **63**, 1–38.

Doulgeris, P., K. Bube, G. Hampson, and G. Blacquire, 2012, Convergence analysis of a coherency-constrained inversion for the separation of blended data: Geophysical Prospecting, **60**, 769–781.

Garcia, D., L. Tarnec, S. Muth, E. Montagnon, J. Poree, and G. Cloutier, 2013, Stolt's f-k migration for plane wave ultrasound imaging: Ultrasonics, Ferroelectrics and Frequency Control, IEEE Transactions on, **60**, 1853–1867.

Garotta, R., 1983, Simultaneous recording of several vibroseis seismic lines: 53rd annual international meeting: 53rd Annual International Meeting, SEG, Expanded Abstracts, 308–310.

Guitton, A., and W. W. Symes, 2003, Robust inversion of seismic data using the huber norm: Geophysics, **68**, 1310–1319.

Hansen, P. C., 1998, Rank-deficient and discrete ill-posed problems: Numerical aspects of linear inversion: Monographs on Mathematical Modeling and Computation, SIAM.

Herrmann, F. J., and G. Hennenfent, 2008, Non-parametric seismic data recovery with curvelet frames: Geophysical Journal International, **173**, 233–248.

Holland, P., and R. Welsch, 1977, Robust regression using iteratively reweighted least-squares: Communications in Statistics-Theory and Methods, **6**, 813–827.

Huber, P. J., 2011, Robust statistics: Springer.

Huo, S., Y. Luo, and P. G. Kelamis, 2012, Simultaneous sources separation via multidirectional vector-median filtering: Geophysics, **77**, V123–V131.

Ibrahim, A., and M. D. Sacchi, 2014a, Accelerating robust Radon transforms via the Stolt operator for simultaneous source separation: 84th Annual International Meeting, SEG, Expanded Abstracts, –.

———, 2014b, Eliminating blending noise using fast apex shifted hyperbolic Radon transform: 76th Annual International Conference and Exhibition, EAGE, Expanded Abstracts, –.

———, 2014c, Simultaneous source separation using a robust Radon transform: Geophysics, **79**, V1–V11.

Ikelle, L., 2010, Coding and decoding: Seismic data: The concept of multishooting: Elsevier Science. Handbook of Geophysical Exploration: Seismic Exploration.

Ji, J., 2006, CGG method for robust inversion and its application to velocity-stack inversion: Geophysics, **71**, R59–R67.

———, 2012, Robust inversion using biweight norm and its application to seismic inversion: Exploration Geophysics, **43**, 70–76.

Kim, Y., I. Gruzinov, M. Guo, and S. Sen, 2009, Source separation of simultaneous source OBC data: 79th Annual International Meeting, SEG, Expanded Abstracts, 51–55.

Li, Z., J. Wang, and Q. H. Liu, 2014, Interpolation-free stolt mapping for SAR imaging: Geoscience and Remote Sensing Letters, IEEE, **11**, 926–929.

Lin, T. T., and F. J. Herrmann, 2009, Designing simultaneous acquisitions with compressive sensing: 71st Annual International Conference and Exhibition, EAGE, Extended Abstracts, S006.

Mahdad, A., P. Doulgeris, and G. Blacquiere, 2011, Separation of blended data by iterative estimation and subtraction of blending interference noise: Geophysics, **76**, Q9–Q17.

Margrave, G. F., 2001, Numerical methods of exploration seismology with algorithms in matlab: The University of Calgary Publ.

Michell, S., E. Shoshitaishvili, D. Chergotis, J. Sharp, and J. Etgen, 2006, Wide azimuth streamer imaging of mad dog; have we solved the subsalt imaging problem?: 76th Annual

International Meeting, SEG, Expanded Abstracts, 2905–2909.

Moore, I., B. Dragoset, T. Ommundsen, D. Wilson, C. Ward, and D. Eke, 2008, Simultaneous source separation using dithered sources: 78th Annual International Meeting, SEG, Expanded Abstracts, 2806–2810.

Radon, J., 1917, Über die Bestimmung von Funktionen durch ihre Integralwerte längs gewisser Mannigfaltigkeiten: Akad. Wiss., **69**, 262–277.

Sacchi, M., and T. Ulrych, 1995a, High-resolution velocity gathers and offset space reconstruction: Geophysics, **60**, 1169–1177.

———, 1995b, Improving resolution of Radon operators using a model re-weighted least squares procedure: Journal of Seismic Exploration, **4**, 315–328.

Sacchi, M., T. Ulrych, and C. Walker, 1998, Interpolation and extrapolation using a high-resolution discrete Fourier transform: Signal Processing, IEEE Transactions on, **46**, 31–38.

Sacchi, M. D., 2014, Sparse inversion of the Radon coefficients in the presence of erratic noise with application to simultaneous seismic source processing: Presented at the 2014 IEEE International Conference on Acoustics, Speech, and Signal Processing (ICASSP), IEEE.

Scales, J., 1987, Tomographic inversion via the conjugate gradient method: Geophysics, **52**, 179.

Stolt, R. H., 1978, Migration by Fourier transform: Geophysics, **43**, 23–48.

Thorson, J. R., and J. F. Claerbout, 1985, Velocity-stack and slant-stack stochastic inversion: Geophysics, **50**, 2727–2741.

Trad, D., 2003, Interpolation and multiple attenuation with migration operators: Geophysics, **68**, 2043–2054.

Trad, D., R. Siliqi, G. Poole, and J. Boelle, 2012, Fast and robust deblending using apex shifted Radon transform: 82nd Annual International Meeting, SEG, Expanded Abstracts, **741**, 1–5.

Trad, D., T. Ulrych, and M. Sacchi, 2003, Latest views of the sparse Radon transform: Geophysics, **68**, 386.

Wason, H., F. J. Herrmann, and T. T. Y. Lin, 2011, Sparsity-promoting recovery from simultaneous data: A compressive sensing approach: 81st Annual International Meeting, SEG, Expanded Abstracts, 6–10.

Wu, J., Z. Li, Y. Huang, J. Yang, and Q. H. Liu, 2014, A generalized omega-k algorithm to process translationally variant bistatic-sar data based on two-dimensional stolt mapping: Geoscience and Remote Sensing, IEEE Transactions on, **52**, 6597–6614.

Yilmaz, O., 2001, Seismic data analysis : processing, inversion, and interpretation of seismic data, 2nd ed.: Society of Exploration Geophysicists. Investigations in geophysics.

LIST OF FIGURES

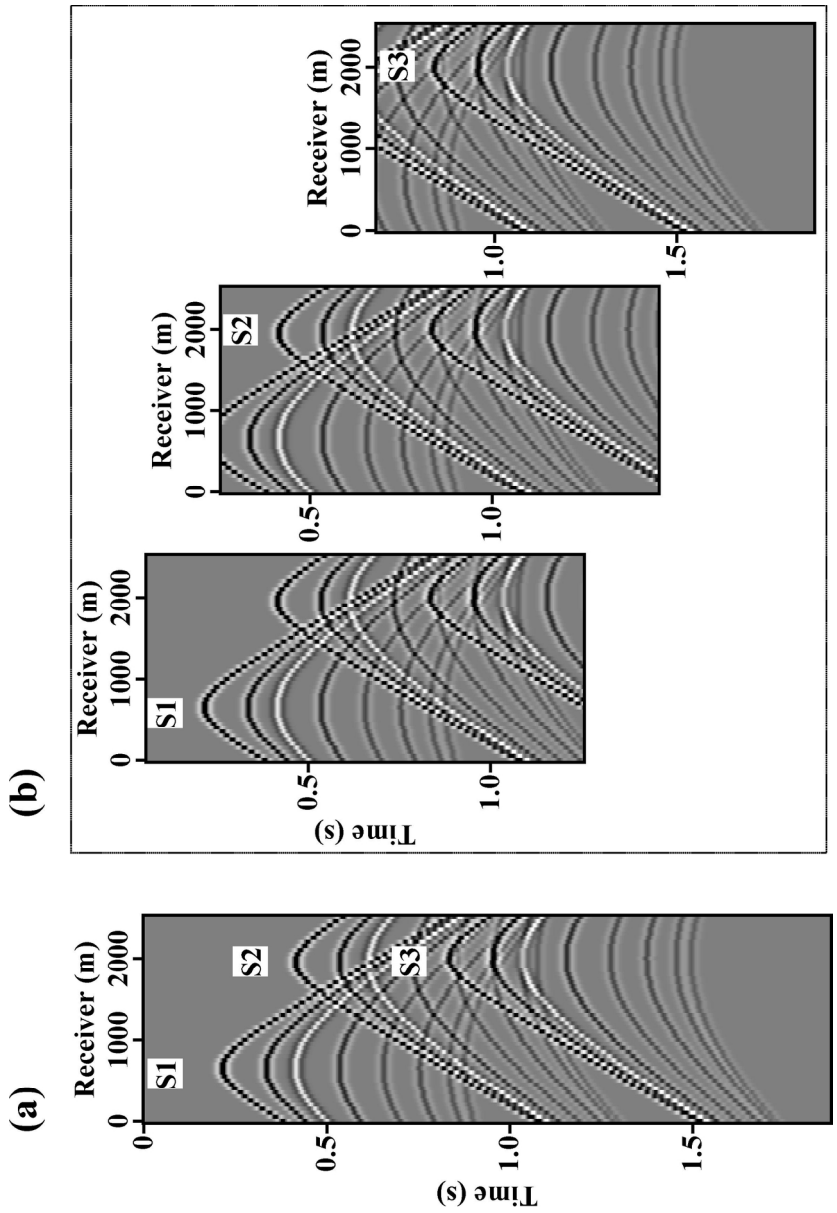

1
146x214mm (300 x 300 DPI)

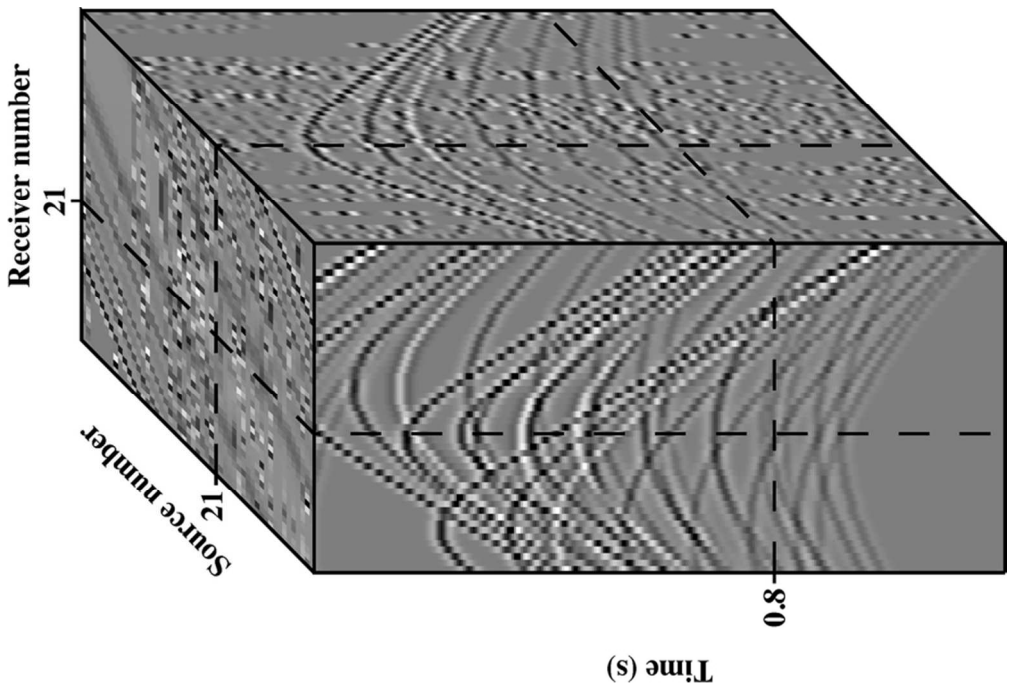

2
78x52mm (300 x 300 DPI)

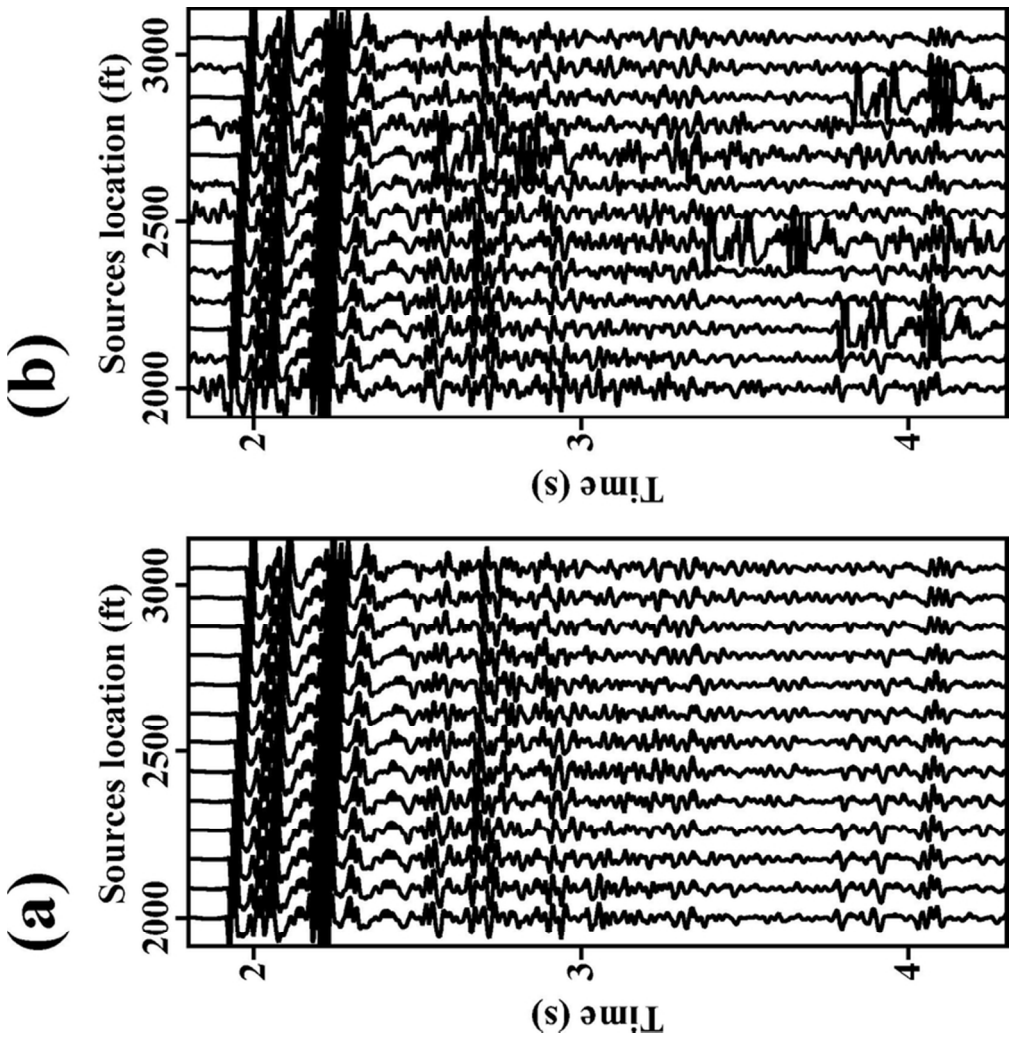

3
71x73mm (300 x 300 DPI)

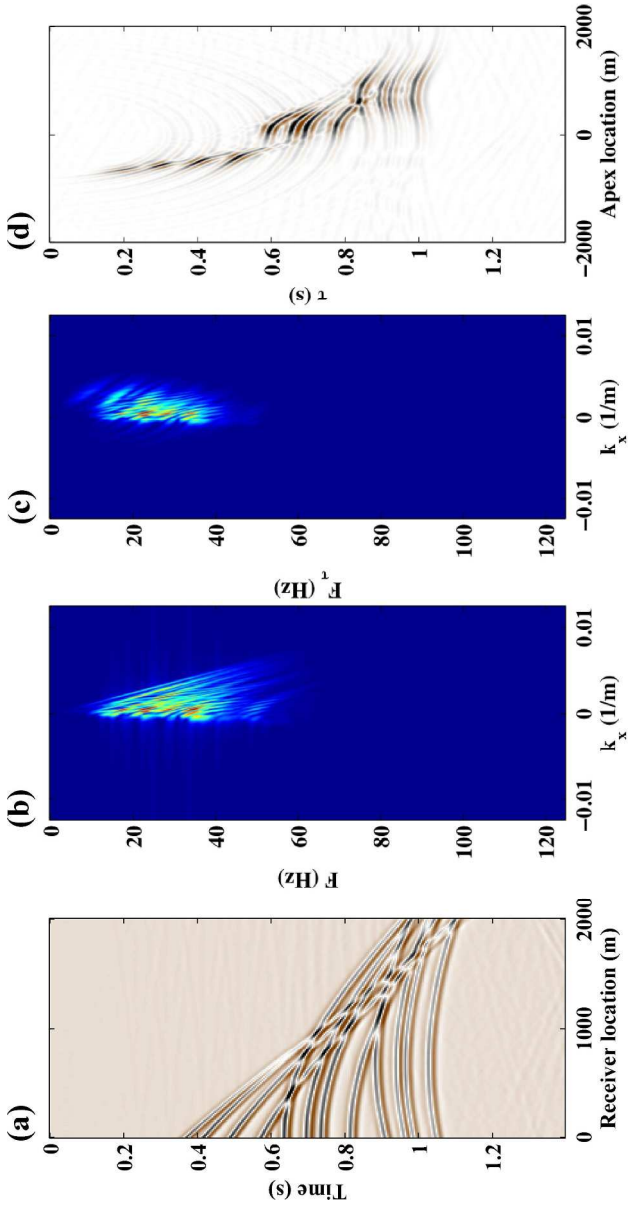

4
187x358mm (300 x 300 DPI)

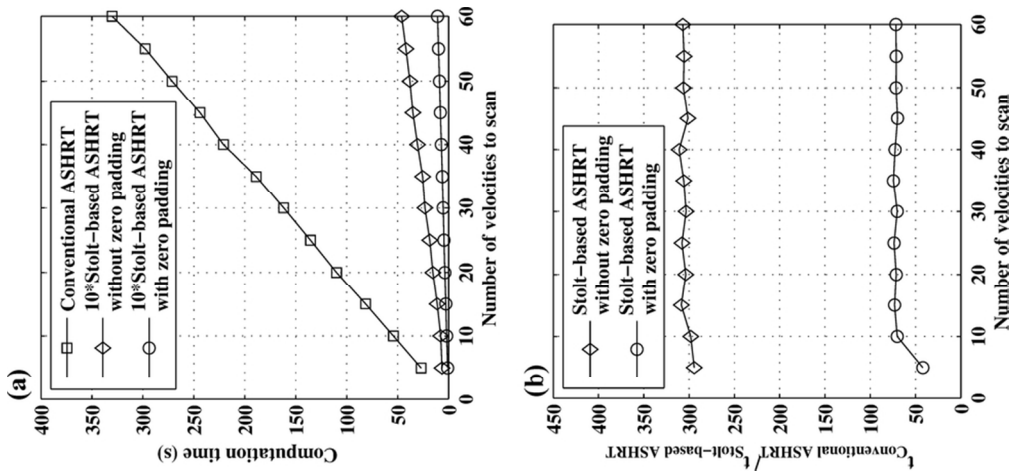

5
82x38mm (300 x 300 DPI)

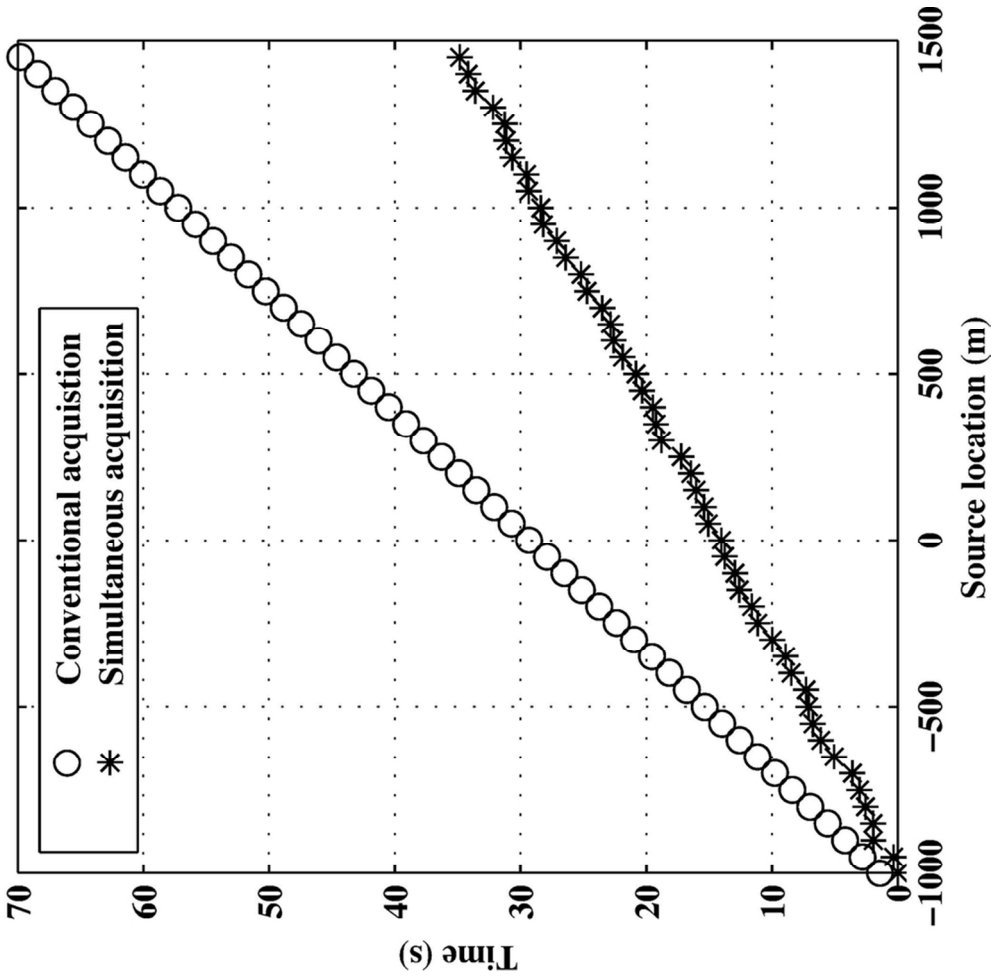

6
85x82mm (300 x 300 DPI)

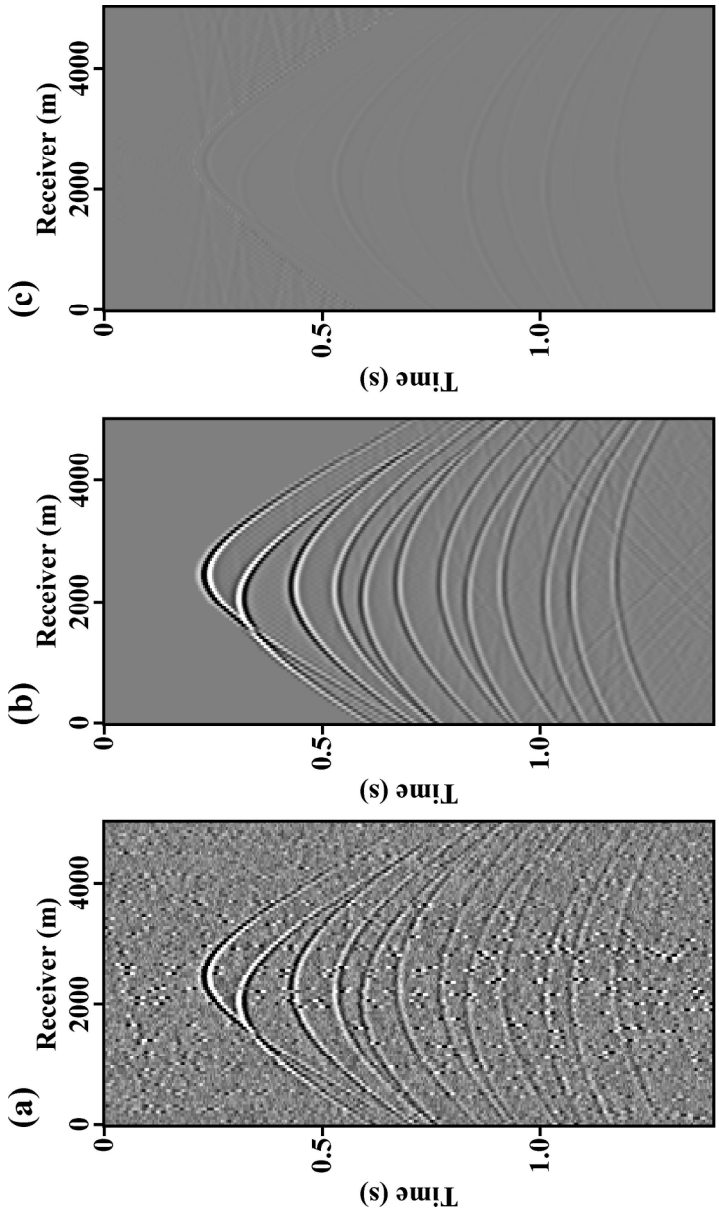

7
167x284mm (300 x 300 DPI)

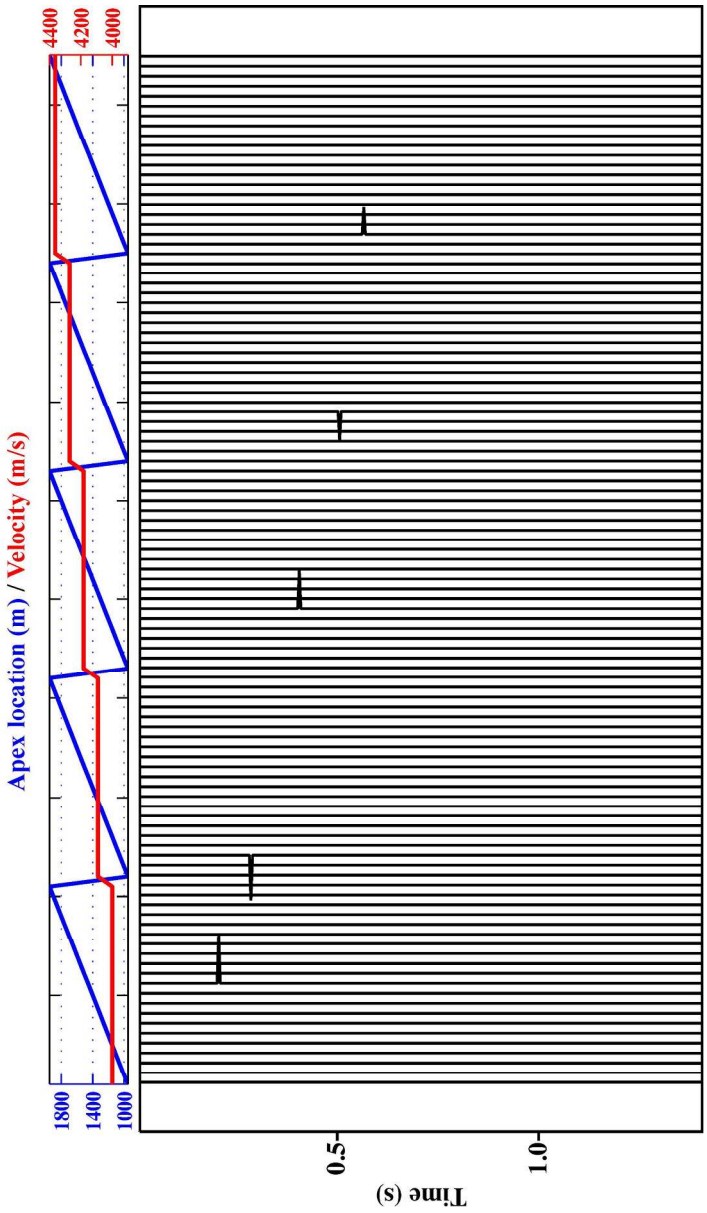

8
166x273mm (300 x 300 DPI)

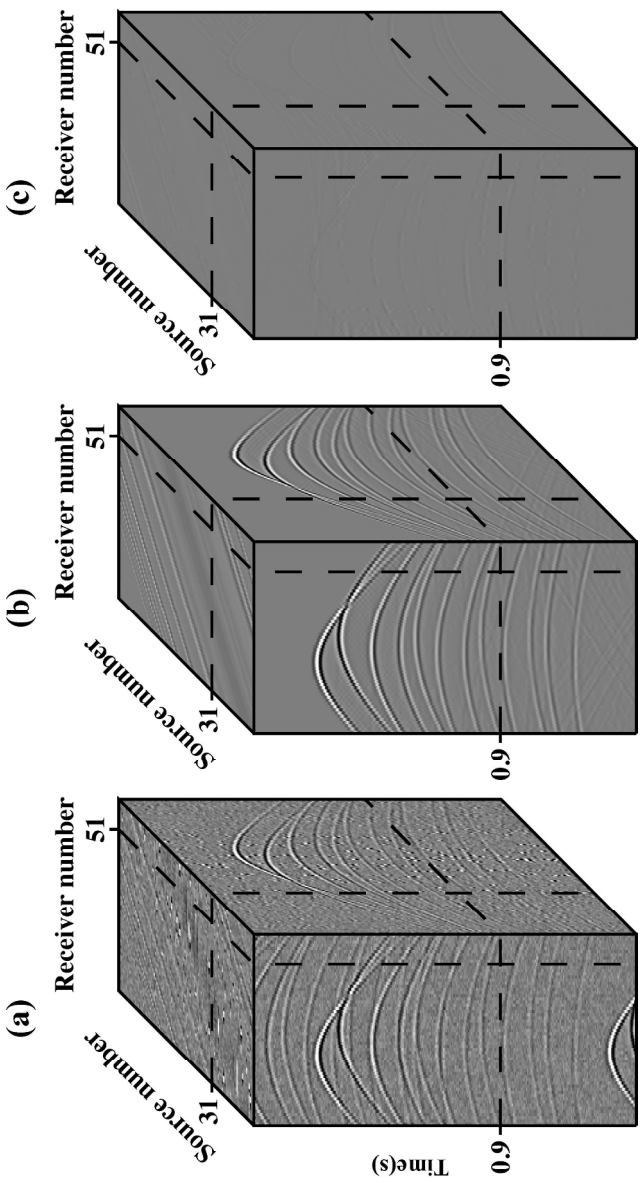

9
177x313mm (300 x 300 DPI)

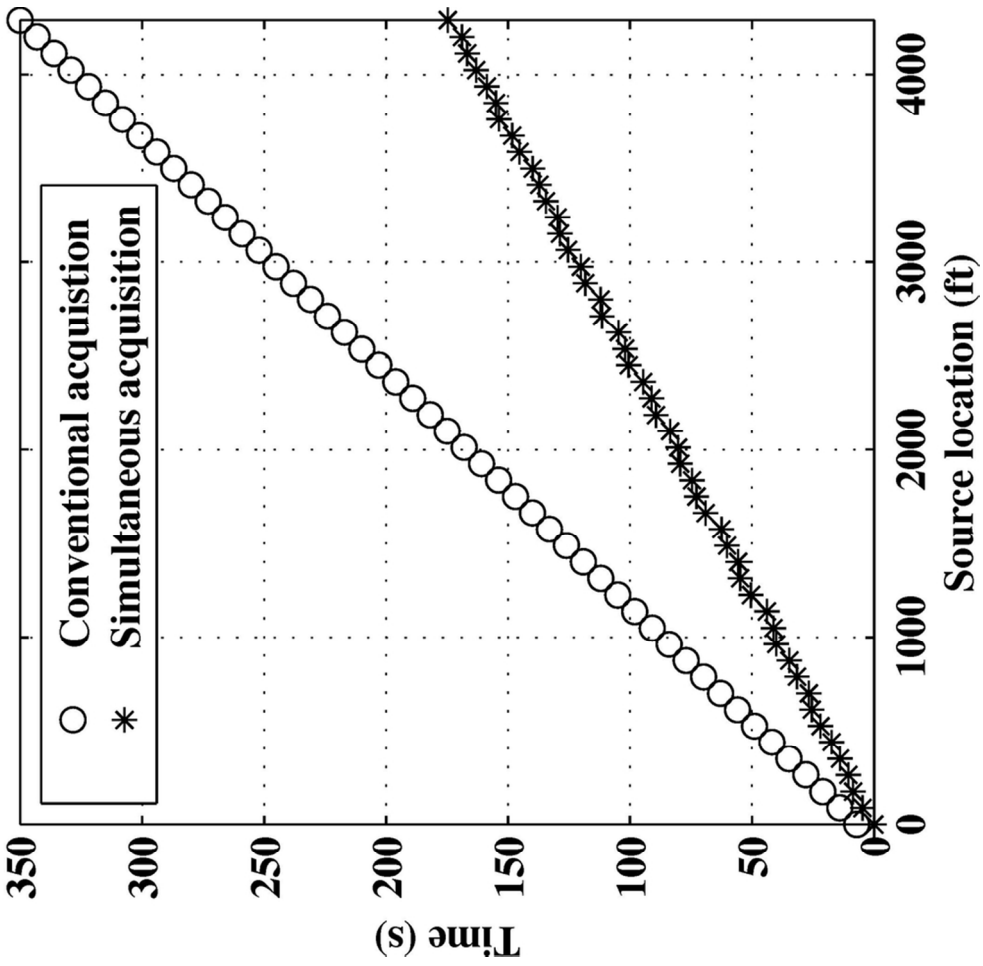

10
86x82mm (300 x 300 DPI)

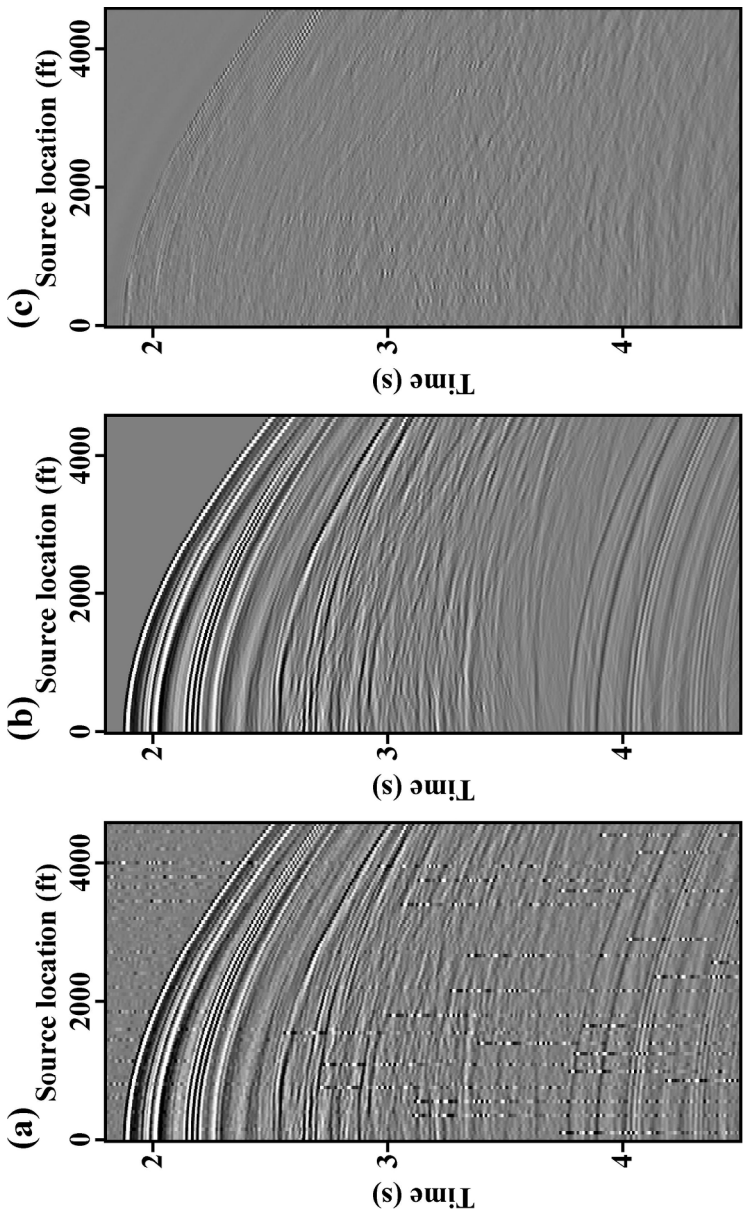

11
162x265mm (300 x 300 DPI)

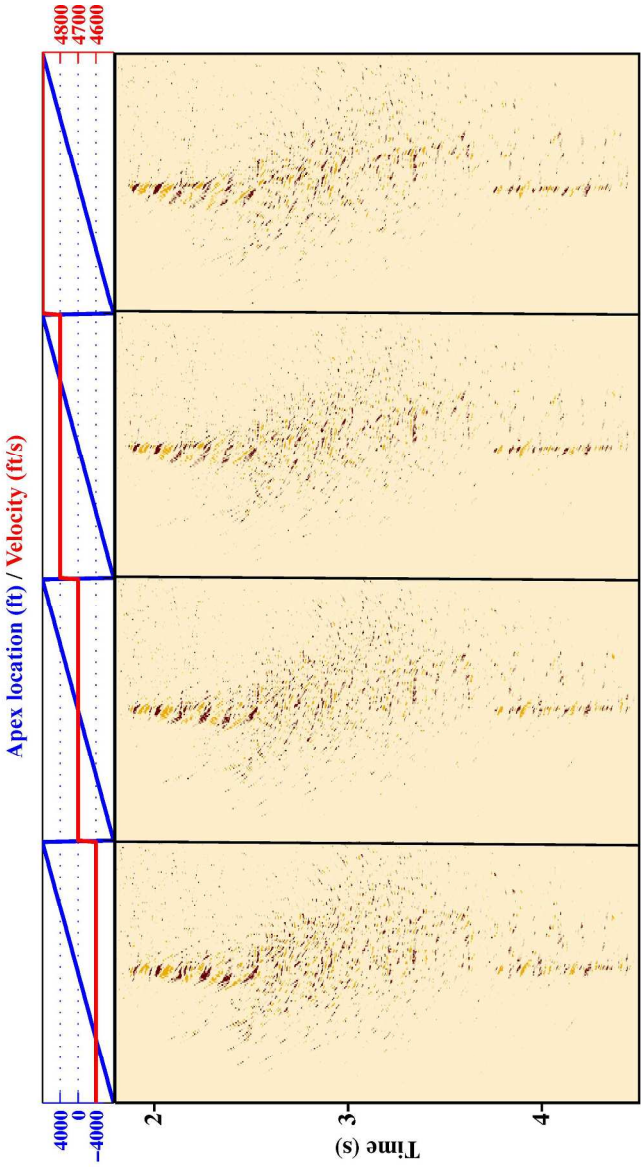

12
181x308mm (300 x 300 DPI)

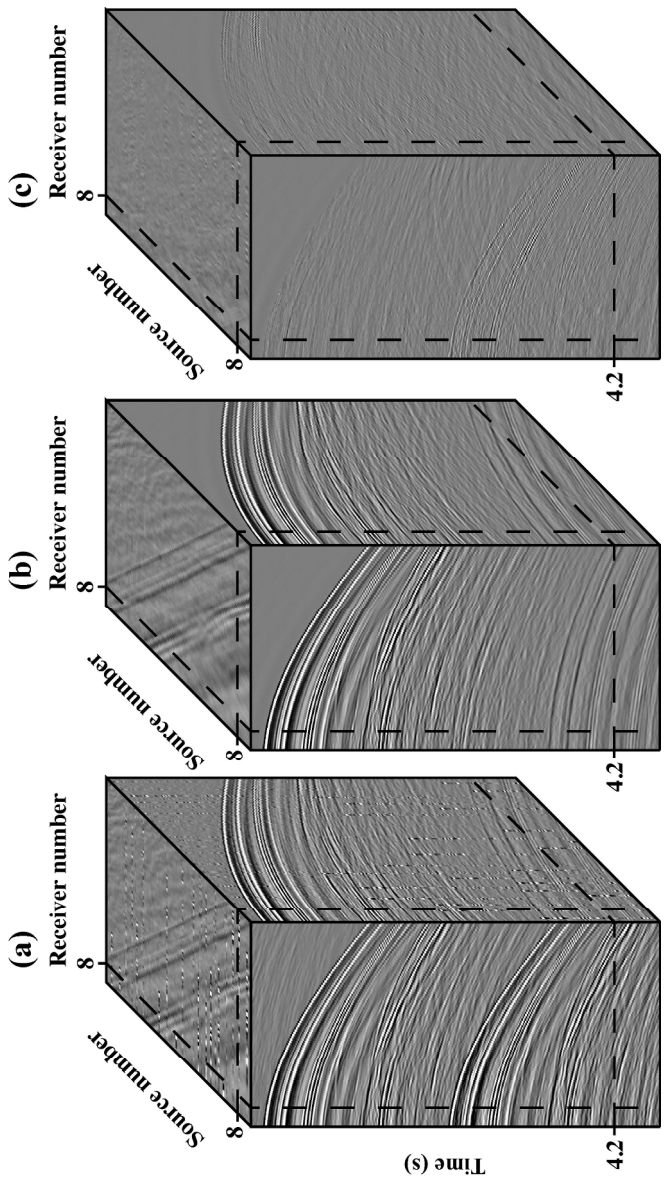

13
181x311mm (300 x 300 DPI)